

# Unfolding designable structures

Cristiano L. Dias\* and Martin Grant†

*Physics Department, Rutherford Building,  
McGill University, 3600 rue University,  
Montréal, Québec, H3A 2T8 Canada*

(Dated: May 24, 2019)

## Abstract

Among an infinite number of possible folds, nature has chosen only about 1000 distinct folds to form protein structures. Theoretical studies suggest that selected folds are intrinsically more designable than others; these selected folds are unusually stable, a property called the designability principle. In this paper we use the 2D hydrophobic-polar lattice model to classify structures according to their designability, and Langevin dynamics to account for their time evolution. We demonstrate that, among all possible folds, the more designable ones are easier to unfold due to their large number of surface-core bonds.

PACS numbers: 87.15.-v, 87.15.Aa, 87.15.By, 87.15.He

---

\*Electronic address: diasc@physics.mcgill.ca

†Electronic address: grant@physics.mcgill.ca

## I. INTRODUCTION

In the human body alone, the number of different proteins is estimated to be in the range of 50,000-100,000 and this number is even larger in the biological world. However, when classified in terms of their three dimensional structures, only 1000 families of protein folds are expected to exist [1, 2]. These structural templates for sequences of amino acids can be explained [3, 4, 5] in terms of minimalistic models where the positions of amino acids are restricted to lattice sites and the interaction energy between residues is described by a coarse-grained model. In this minimalistic approach, structures are classified according to their designability, *i.e.* the number of amino acid sequences they can accommodate. While some structures are not used to describe proteins, *i.e.* their designability is zero, a few structures are designed by an enormous number of sequences and are, therefore, stable to amino acid mutation – a desirable and natural feature for evolution. Also, highly designable structures emerge as being thermodynamically stable [3] and having protein-like symmetry [3, 4, 6].

Designability has also been shown to have dynamical implications: calculations suggest [7] that sequences of amino acids that fold into highly designable structures, and are thermodynamically stable, present a faster folding kinetics than random sequences – as expected for real proteins. Another important dynamical aspect of proteins is their reaction to external force fields: in their natural environment, proteins have to cope with forces during their activities. It might be expected that the set of structures which constitute recurring protein folds react differently to forces than other folds. In this paper we confirm this expectation. We study the dependence of the phase diagram on designability and show that *for any combination of temperature and shear, high-designable structures are the easiest structures to unfold*. This result is a consequence of how the backbone (involving strong covalent bonds) and weak bonds are distributed in these structures.

This article is organized as follow: below we review the relation between designability, thermodynamic stability and surface-to-core bonds. Following this, the model to study unfolding is introduced, together with the mathematical framework to characterize this process. Results are then presented, followed by a discussion.

## II. DESIGNABILITY

The relation between designability and thermodynamical stability has been studied extensively with the hydrophobic-polar (HP) model and some of its variants in a square and cubic lattice [3, 8, 9] and in a 3-state off-lattice model [5]. The goal of this section is to review this relation for the HP model in the two-dimensional compact triangular lattice for which little is known [10] and which describes equilibrium structures of our protein model in the next section. The HP model of protein folding is believed to contain the essential ingredients for the designability problem.

In the HP model [11] a protein is considered to be a chain made of polar (P) and hydrophobic (H) like amino acids. Hydrophobicity is the only aspect of amino acids which is taken into account since it is considered the main driving force for folding [12, 13]. In this coarse-grained approach the energy of a sequence folded into a structure is given by the short-range contact interaction:

$$\mathcal{H} = \sum_{i < j} \epsilon_{i,j} \left[ \delta(|\vec{r}_i - \vec{r}_j| - \sigma) - \delta_{j-1,i} \right] \quad (1)$$

where  $\vec{r}_i$  is the position of the  $i$  monomer and  $\sigma$  is distance between lattice sites. The first delta function allows only nearest-neighbors interaction and the second delta excludes interaction between residues which are adjacent along the backbone. The interaction energy between monomers  $i$  and  $j$ ,  $\epsilon_{i,j}$ , can assume 3 values depending on the type of monomers bounded: H-H, H-P, P-P. These values are chosen to minimize the Hamiltonian when H like amino acids are buried inside the protein and P like amino acids are left on the surface. This is achieved whenever  $\epsilon_{PP} > \epsilon_{HP} > \epsilon_{HH}$ . To account for the segregation of different types of amino acids an additional condition has to be imposed  $2\epsilon_{HP} > \epsilon_{PP} + \epsilon_{HH}$ . Since compact shapes have maximum contact and therefore have the lowest energy states, they are the only shapes considered for representing proteins. With this simplification, the interaction energies can be shifted without changing the relative energies of a sequence when folded in different conformations. Following Li *et al* [3], we use:  $\epsilon_{HH} = -2.3$ ,  $\epsilon_{HP} = -1$  and  $\epsilon_{PP} = 0$ . These values are given in arbitrary units.

In this work, proteins are 25 amino acids long and the different structures they can assume are restricted to compact self-avoiding walks on a 5 X 5 triangular lattice – see Fig. 1(d) for an example of structure. The number of independent structures that can be formed under

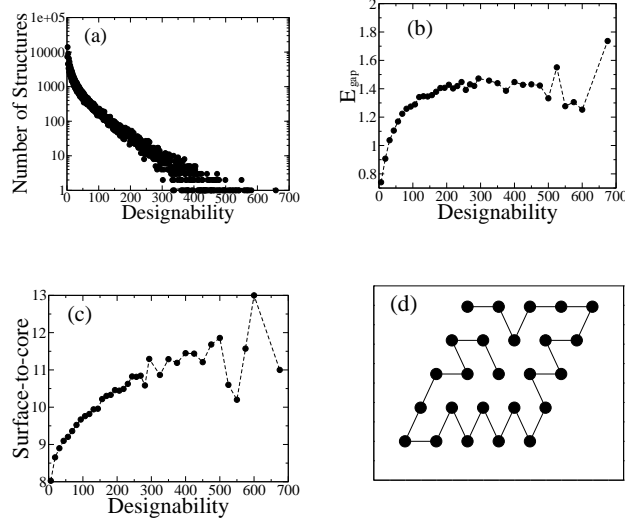


FIG. 1: a) Histogram of designability. b) Dependence of energy gap on designability. c) Number of bond connecting surface to core residues versus designability. d) Fifth most designable structure.

these conditions is 352,375. Now, given a sequence of amino acids, each structure can be scanned for its native state – *i.e.* its non-degenerate ground state. Sequences with degenerate ground states are believed to be unrealistic since their native states are not well defined. These sequences are therefore ignored. For our small protein, the ground state of all its  $2^{25}$  binary sequences can be computed and we count the number of sequences that fold uniquely into a structure. This number corresponds to the designability of the given structure. We find that among the 352,375 structures only 135,216 ( $\sim 38\%$ ) are non-degenerate ground states of at least one sequence.

The distribution of designability for the 135,216 structures is given in Fig. 1(a). Compact structures are very different when it comes to designability: many structures have a low value of designability, while just a rare number of folds accommodate more than 500 sequences. These high-designable structures are on average more stable thermodynamically than other structures. This can be shown by computing the energy difference between the ground state  $E_o$  and the first excited state  $E_1$  of a sequence:  $E_{gap} = E_1 - E_o$ . This energy difference is then averaged over sequences that have the same ground state and it is a measure of the stability of the given ground state. The correlation between  $E_{gap}$  and designability is given in Fig. 1(b) where  $E_{gap}$  is averaged over a given range of designabilities.

A geometrical property of these selected structures is the large number of bonds connect-

ing surface monomers to core monomers [6, 14, 15, 16]. This is illustrated in Fig. 1(c) where the number of bonds connecting surface to core, averaged over structures of a given range of designability, is plotted against designability. A systematic increase of surface-to-core bonds with designability is observed. An example of structure which has a large number of bonds connecting surface to core residue is the fifth most designable structure - shown in Fig. 1(d).

### III. MODEL

In the previous section we have shown that the surface of high-designable structures is differently connected to the core of the protein when compared to the surface of low-designable structures – Fig. 1(c). Therefore, since unfolding starts by unbinding surface monomers from the core, it might be expected that the dynamics of unfolding depends on designability. To investigate this idea, we present in this section a model to probe the dynamics of structures in the presence of applied forces.

In this model, the energy of each structure is accounted for by two types of potentials: monomers which are adjacent along the backbone of the protein interact through a harmonic potential otherwise the interaction is via a Lennard-Jones potential. The harmonic bond ensures that the backbone of the protein is preserved during the simulation while monomers bound by a Lennard-Jones potential can be driven apart, changing the structure of the protein. In this way, the potential energy of the chain is:

$$V(r_{i,j}) = \sum_{i=1}^{N-1} \frac{k}{2} (r_{i,i+1} - \sigma)^2 + \frac{1}{2} \sum_{\substack{j \neq i \pm 1 \\ j \neq i}} \epsilon \left[ \left( \frac{\sigma}{r_{i,j}} \right)^{12} - 2 \left( \frac{\sigma}{r_{i,j}} \right)^6 \right] \quad (2)$$

in the last sum,  $i$  and  $j$  range from 1 to  $N$  and  $r_{i,j}$  is the distance between monomers  $i$  and  $j$ .  $\epsilon$  and  $\sigma$  are the binding energy and equilibrium length of monomers. A cut-off distance of  $2.5\sigma$  is used for the Lennard-Jones potential and  $k$  is the spring constant of the harmonic potential. Notice that the model does not discriminate between P and H amino acids such that the dynamics of unfolding can be related directly to the topology of the native structure independently of amino acids sequences.

The equilibrium length of the harmonic and the Lennard-Jones potentials are the same such that the minimal energy structure of the model in two dimensions is (to small corrections due to surface effects) a triangular lattice. So each of the 135,216 designable structures

described in the previous section corresponds to a local minima of energy and can be viewed as *equilibrium structures*. Notice that these native states are degenerate such that no structure is preferred over others. However this degeneracy can be removed if a field is applied. This is what we do next by coupling the protein model to a fluid flow.

The fluid is modeled by including a friction and a random term  $f_i(t)$  to the force acting on each monomer (Langevin dynamics). The intensity of the random force is given by the fluctuation-dissipation theorem. The friction force on each monomer is proportional to the relative velocity of the monomer with respect to the fluid:  $-\gamma \vec{v}_{rel}$  ( $\gamma$  is the friction coefficient). For the velocity of an element of the fluid located at position  $\vec{r}$ , *i.e.*  $\vec{r} = x \hat{x} + y \hat{y}$ , we use the velocity profile:  $\vec{v}_{fluid}(\vec{r}) = Sy \hat{x}$ , where  $S$  is the shear rate. Inside such a fluid flow, an extended elastic object rotates and gets stretched with an intensity dependent on its orientation with respect to the fluid flow.

Putting the forces that act on a monomer together, its equation of motion inside the elongational flow is:

$$M \frac{d^2 \vec{r}_i}{dt^2} = \sum_j \vec{F}(r_{ij}) - M\gamma[\dot{\vec{r}}_i - \vec{v}_{fluid}(r)] + \vec{f}_i(t) \quad (3)$$

where  $\vec{r}_i$  and  $\dot{\vec{r}}_i$  are the vectors representing the position and velocity of monomer  $i$ . Here,  $M$  is the mass of a monomer,  $\vec{F}$  is the force computed from the interacting potential. For simplicity,  $\sigma$ ,  $\epsilon$  and  $M$  are chosen to be one. The spring is chosen to be five times stiffer than the Lennard-Jones potential:  $k = 5(72\epsilon/\sigma^2)$ . Simulations are carried out in units of the fastest atomic vibration:  $\tau_o = 2\pi\sqrt{k/M}$ ; and the friction constant is given a value of:  $\gamma = (\tau_o/4)^{-1}$ .

## IV. SIMULATING UNFOLDING

### A. Methodology

In this section we describe how simulations are carried out and how we characterize the unfolding process. As the initial structure of our protein, we choose one of the 135,216 structures formed on the compact triangular lattice. Initial velocities are chosen according to a Maxwell-Boltzman distribution at a given temperature  $T$ . Time evolution of the initial configuration is obtained by solving numerically equation 3 – we use the velocity-Verlet

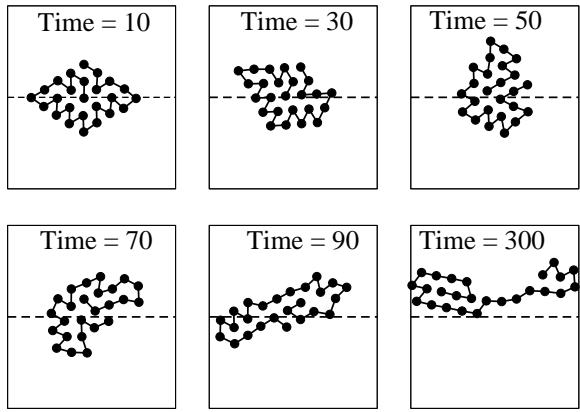


FIG. 2: Snapshot of beads position during unfolding. This simulation was performed at a temperature of 0.20 (in units of  $\epsilon$ ) and using a velocity gradient of 0.26. The position of zero velocity flow is represented by a dotted line in these panels.

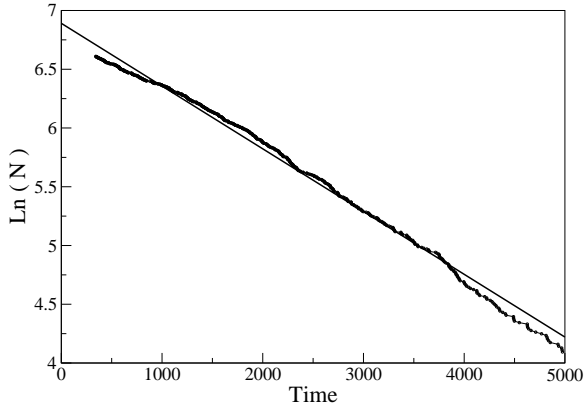


FIG. 3: Natural logarithm of the number  $N(t)$  of folded chains as a function of time. Here  $T = 0.30$  and  $S = 0.10$ . The straight line is a best-fit line – which gives  $\tau = 1872.7679$ .

algorithm for this purpose [17]. As a sample calculation, we illustrate in Fig. 2 the unfolding of the fifth most designable structure. This simulation is performed at a temperature of 0.20 (in units of  $\epsilon$ ) and a velocity gradient for the fluid flow of 0.26. In the first and second panel of 2 the initial structure is preserved while the molecule rotates. Many bonds rupture in the following panels such that the structure at time  $70\tau_o$  has lost all its resemblance to the initial state.

Since unfolding occurs through the rupture of bonds we quantify the unfolding process by the mean coordination of the chain: a folded chain has a coordination of approximately 4.5 while the coordination of an unfolded chain is approximately 2. The velocity profile used in this work does not provide a constant driving force for unfolding. So, the molecule undergoes many cycles of partial unfolding followed by folding. Since our main interest is to compare how the dynamics of unfolding depends on the initial structure there is no point in studying the system at latter times (when the initial structure is strongly deformed). Therefore we study the system until five bonds rupture (when the coordination of the chain is 4.08). The quantity of interest is the mean time  $\tau$  required to bring the system, for the first time, from a folded configuration into a state with five broken bond. This time will be called *unfolding time*. Quantitatively, the time of unfolding is sensitive to the criteria for defining unfolding. However the qualitative trend, which is of interest here, does not depend on this definition. To compute the mean coordination, a bond is defined whenever the distance between two atoms is less than  $1.5\sigma$ .

Due to the stochastic nature of unfolding we use  $N_o = 800$  chains when computing the characteristic unfolding time. The initial relative positions of beads in each of these chains are the same. However chains are rotated by  $2\pi/N_o$  with respect to each other such that each chain has a different orientation compared to the direction of fluid flow. Rotation is performed while keeping the center of mass of the molecule in the line of zero velocity flow. In a simulation all chains unfold as time evolves. It might be expected that the number of chains that unfold at time  $t$  ( $dN/dt$ ) is proportional to the population of folded chains  $N(t)$ . In this case,  $N(t) = N_o \exp(-Rt)$  where  $R$  is the rate of unfolding. A typical simulation, performed at a temperature of 0.20 and a velocity gradient of 0.25, confirms this behavior in Fig. 3. It is straightforward to compute  $R$  in this framework: it corresponds to the slope of the line in Fig.3. Notice that the characteristic unfolding time  $\tau$  is given by the inverse of the rate  $\tau = 1/R$ .

## B. Unfolding time

The dependence of  $\tau$  on the different simulational parameters is now studied. The logarithm of  $\tau$  is shown in Fig. 4 for different  $\beta = 1/kT$  and different shear rates ( $S$ ). For a given velocity gradient,  $\tau$  increases exponentially with  $\beta$ . This characterizes thermally-activated

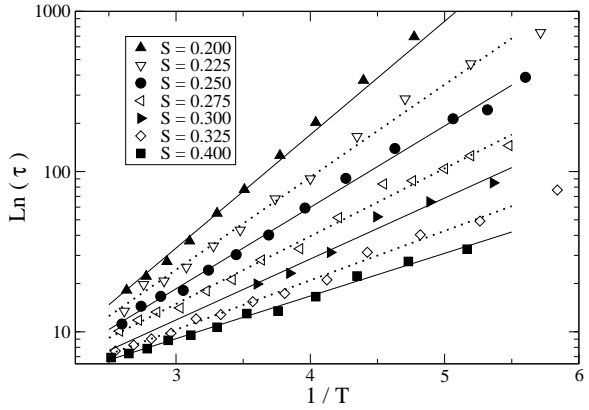


FIG. 4: Dependence of the time of unfolding on the inverse of temperature. Different symbols correspond to different shear rates. Lines correspond to linear fit.

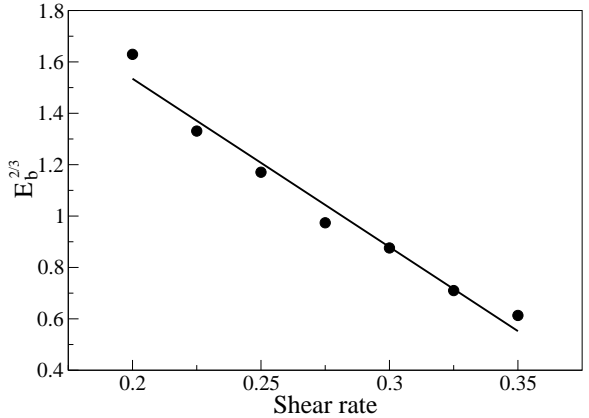


FIG. 5: Dependence of the energy barrier on the shear rate.

processes for which:

$$\tau = \frac{1}{\Omega} \exp(E_b/kT). \quad (4)$$

In this equation,  $E_b$  and  $\Omega$  correspond respectively to the energy barrier the system has to overcome before unfolding can start and the trial frequency of this process. Thus, in order to characterize how a structure resist a given velocity gradient we need to determine both  $E_b$  and  $\Omega$ .

In the language of transition state theory [18] the folded chain corresponds to a metastable state which has to overcome an energy barrier to reach other minima. The average path between two minima is quantified by a reaction coordinate  $\phi$ . As the shear rate increases, the

energy barrier decreases and vanishes at a critical gradient  $S_c$ . At this critical gradient the fixed point  $\phi_-$ , corresponding to the metastable state, and the fixed point  $\phi_+$ , representing the top of the barrier, fuse into an inflection point  $\phi_c$ . An analytical expression for the dependence of the energy barrier on the shear rate can be obtained for  $(1 - S/S_c) \ll 1$ . For simplicity,  $\tilde{\phi} \equiv (1 - \phi/\phi_c)$  and  $\tilde{s} \equiv (1 - S/S_c)$ .

At the inflection point  $(\partial E/\partial \tilde{\phi}_c)_{\tilde{s}_c} = (\partial^2 E/\partial \tilde{\phi}_c^2)_{\tilde{s}_c} = 0$  – such that the energy barrier for  $\tilde{s}_c \ll 1$  and  $\tilde{\phi}_c \ll 1$  is:

$$E_b(\tilde{\phi}_+, \tilde{s}) = E(\tilde{\phi}_+, \tilde{s}) - E(\tilde{\phi}_-, \tilde{s}) \quad (5)$$

$$\simeq A\tilde{\phi}_+^3 - B\tilde{\phi}_+\tilde{s} \quad (6)$$

where we used  $\tilde{\phi}_+ \simeq -\tilde{\phi}_-$ . Equation 6 has not the desired form yet since the barrier depends on both  $\tilde{s}$  and  $\tilde{\phi}_+$ . The dependence on  $\tilde{\phi}_+$  can be removed by solving  $(\partial E/\partial \tilde{\phi}_+)_c = 0$  to lowest order in  $\tilde{s}$  and  $\tilde{\phi}$ , yielding:

$$\tilde{\phi}_+ \simeq Cs^{1/2}. \quad (7)$$

The energy barrier can now be obtained as a function of  $\tilde{s}$  only:

$$E_b(\tilde{s}) \simeq E_o \tilde{s}^{3/2} \quad (8)$$

where  $A, B, C$  are constants and  $E_o$  is an energy parameter. The scaling given by the last equation is found in different context where the important fixed point of the energy surface is an inflection point [19]. Examples are atomic friction [20], Josephson tunnel junctions [21] and force spectroscopy [22, 23]. In Fig. 5 we illustrate the dependence of  $E_b$  on the velocity gradient. These quantities were extracted by fitting the data of Fig. 4 according Eq. 4. Axis are chosen such that data obeying equations 8 will fall into a straight line. The energy barrier is well described by equation 8 and a linear fit gives  $E_o$  and  $S_c$ .

## V. RESULTS

Now we quantitatively evaluate how structures with differing designabilities react to both thermal fluctuations and an applied shear force. Rather than simulate all 135,216 structures, we sample as follows. We study all the 1500 structures with highest designability, ranging from 200 to 700. For the more numerous structures which are less designable, we consider eight randomly-chosen structures for each designability. This ensemble of 3100 structures is representative of the diversity of folds.

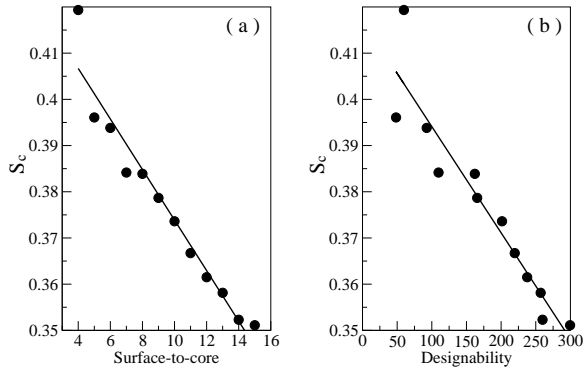


FIG. 6: (a) Dependence of the critical velocity flow on the number of surface-core bonds. (b) The dependence of  $S_c$  on the average designability of structures having the same number of surface-core bonds. Lines in these figures are just a guide to the eye.

### A. Shear induced unfolding

Here we study how structures differing in designability react to an applied shear force. This is done following Eq. 8. The two parameters of this equation  $E_o$  and  $S_c$  can in principle be computed and used to discriminate between structures. However for practical reasons we only compute  $S_c$  in this work.

At zero temperature, a structure only unfolds if the shear rate is greater than  $S_c$  - *i.e.* when the barrier is zero. Therefore if (at zero temperature) a structure does not unfold at a given  $S_o$  but unfolds at  $S_o + \delta$ , the critical shear  $S_c \equiv S_o + \delta/2$ .  $\delta$  being a numerical parameter accounting for the precision of the calculation. To be statistically significant we probe eight copies of each structure to different values (all differing by  $\delta = 0.001$ ) of the velocity flow – each copy having a different orientations with respect to the fluid. In order to certify that the chosen simulational time (about 5,000 atomic vibration) is not affecting significantly the calculation of  $S_c$ , a few structures were subjected to twice that time. Since no significant variations of  $S_c$  was observed, our choice of simulational time seems to be a good compromise between computational expense and precision.

We note that unfolding starts at the surface, where monomers are less bound (their coordination is lower). In particular a structure which has a backbone connecting many surface to core monomers is especially sensitive to an applied force since this structure

contains many small domains at the surface which are weakly bound to each other. In contrast, if the backbone connects many surface monomers together before binding them to the core, only large forces will be able to produce unfolding since many weak bonds have to break to separate surface from core. This idea is confirmed in Fig. 6(a) where the dependence of  $S_c$  on the number of times the backbone connects a surface to a core monomer is shown. *Structures with a backbone zigzagging many times between surface and core are sensitive to small gradients in contrast to more linear backbone structures.*

In Fig. 6(b) we illustrate the dependence of  $S_c$  on designability. In this Figure, both  $S_c$  and designability has been averaged over structures having the same number of surface-to-core bonds. *A clear correlation between these quantities indicates that structures which are highly designable require less shear to unfold.*

We note that the critical velocity gradient of a high and low designable structure differed by at most 10% - see Fig. 6. Although such a variation of the gradient does not seem important, its effect on the energy barrier is very significant. For example, if we probe two structures, for which  $S_c$  are 0.4 and 0.35 respectively, to a flow described by a velocity gradient of 0.3 – then, according to equation 8, the energy barrier of these structures will be 0.25 and 0.10 respectively (supposing  $E_o = 2$  for both structures). Therefore an increase of only  $\sim 10\%$  in the critical velocity flow causes the energy barrier to double. This is a significant effect which affects exponentially the unfolding time of a protein (see Eq. 4).

## B. Thermal induced unfolding

In this subsection we are concerned with thermally induced unfolding. Therefore the shear rate of our model is set to zero such that the only cause of unfolding is thermal fluctuations. Unfolding is illustrated in Fig. 7. The upper (lower) panels of this Figure correspond to the unfolding of a low (highly) designable structure. These simulations were performed at a temperature of 0.70 (in units of  $\epsilon$ ). Low designable structures have few surface to core bonds. As a result, many weak bonds are aligned forming domains (or sub-structures) where monomers are correlated over long distances. For those structures, the time of unfolding is dominated by the slow unbinding of the largest domain. In contrast, high designable structures are formed by many small domains which are approximately of the same size. Here, unfolding occurs concurrently at many of these domains. Therefore, one should expect

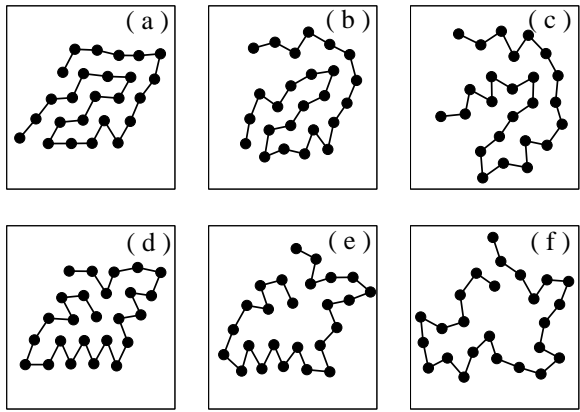


FIG. 7: Snapshot of a low (panels *a*, *b* and *c*) and a highly (panels *d*, *e* and *f*) designable structure during thermally induced unfolding ( $S = 0$  and  $T = 0.70$ ). Panels *a* and *d* show beads position at time  $\tau_o$  and a time interval of  $15 \tau_o$  has elapsed between each panel.

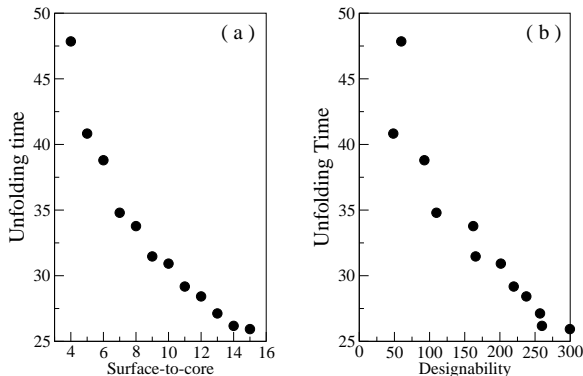


FIG. 8: Dependence of the unfolding time on (a) number of surface-to-core monomers and (b) designability.

highly designable structures to be less resistant to thermal fluctuations than low designable ones. This is confirmed qualitatively in Fig. 7: for the low designable structure, the largest domain is still preserved after  $30 \tau_o$  (panel *c*) while for the high designable structure all the small domains have been destroyed (panel *f*).

To verify this hypothesis quantitatively, we compute the unfolding time of the ensemble of 3100 structures at a temperature of  $0.50$  (in units of  $\epsilon$ ) and zero shear rate – see Fig. 8. The larger the unfolding time of a structure, the more stable it is to thermal fluctuations. In Fig. 8(a) the unfolding time is plotted versus the number of surface-to-core bonds. The clear

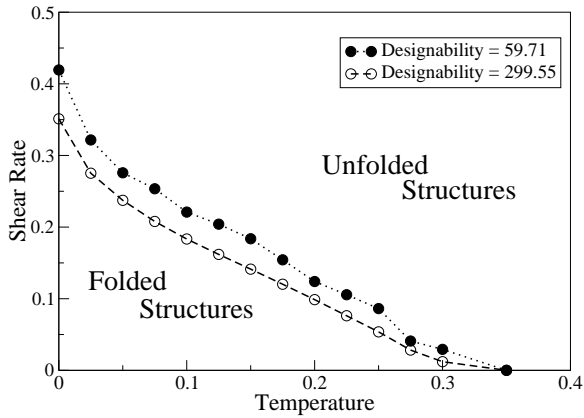


FIG. 9: Phase diagram of the set of structures having 4 and 15 surface-to-core bonds – filled and open circles, respectively. The latter (former) has an average designability of 299.55 (59.71).

downward trend of this figure indicates that *structures with many surface-to-core bonds, and therefore with many small domains, unfold faster*.

Figure 8(b) presents the correlation between unfolding time and designability. This Figure was obtained by averaging both time of unfolding and designability over structures having the same number of surface-to-core bonds. Again a clear correlation indicates that on average, *structures with low designability are more robust to thermal fluctuations*.

### C. Designability dependent phase-diagram

We now study how the designability of a protein affects its phase-diagram. This diagram is constructed by computing the applied shear rate required to unfold a structure in 5,000 units of time at different temperatures. This shear rate is then averaged over structures having the same number of surface-to-core bonds. Notice that the computed shear delimits two regions of the diagram: folded structures are found below this shear and unfolded structures above it. In Fig. 9 the phase-diagram is shown for structures having 4 and 15 surface-to-core bonds. These two sets of structures have an average designability of 59.71 and 299.55 respectively. At any temperature, the set of structures with lower designability is more robust and require a higher shear rate to unfold. *One can therefore state that high designable structures are easier to unfold than low designable ones.*

## VI. DISCUSSION

The relation between thermodynamical stability and designability, called the designability principle, has been shown in Fig. 1(b): the energy difference between the ground state and the first excited state, averaged over all sequences having the same ground state, increases with the designability of the ground state. Therefore, close to equilibrium, the probability of finding a sequence in its native structure – as opposed to other compact configurations – is proportional to the designability of the native structure. In other words, highly designable structures are more stable thermodynamically than low designable ones.

In marked contrast to the designability principle, we have shown that highly designable structures are easier to unfold than low designable ones – *i.e.* they are weaker. The implication is that, although highly designable structures are more stable in the folded region of the phase diagram, they require less perturbation to unfold. We speculate this may be related to protein flexibility.

A qualitative explanation is as follow. We have shown that highly designable structures are weaker due to the large number of surface-to-core bonds they contain: as a result of this feature, structures contain many small domains. These are easy to unfold, *i.e.* only a few bonds need to rupture, and they unfold concurrently as one approaches the region of the phase diagram where folded structures become unstable. Also, the presence in large number of surface-to-core bonds makes it difficult to transform highly designable structures into other distinct compact shapes through local rearrangements of the backbone [4]. Such an unlikely transformation, at least in the region of the phase diagram where folded structures are at equilibrium, would require the partial unfolding of the structure followed by folding into the new shape. Therefore, the presence of surface-to-core bonds might explain why high designable structures are thermodynamically stable but easier to unfolding. Finally, we expect interesting insights to be obtained by expanding the model to three dimensions and including hydrodynamics effects (*i.e.* modeling the solvent explicitly).

## VII. ACKNOWLEDGEMENT

CLD would like to thank Anirban Sain and Markus Miettinen for insightful discussions. This work was supported by the Natural Sciences and Engineering Research Council of

Canada, and *le Fonds Québécois de la recherche sur la nature et les technologies*.

---

- [1] S. E. Brenner, C. Chothia, and T. J. Hubbard, *Current Opinion in Structural Biology* **7**, 369 (1997).
- [2] A. G. Murzin, S. E. Brenner, T. Hubbard, and C. Chothia, *Journal of Molecular Biology* **247**, 536 (1995).
- [3] H. Li, R. Helling, C. Tang, and N. Wingreen, *Science* **273**, 666 (1996).
- [4] H. Li, C. Tang, and N. S. Wingreen, *Proc. Natl. Acad. Sci. USA* **95**, 4987 (1998).
- [5] J. Miller, C. Zeng, N. S. Wingreen, and C. Tang, *PROTEINS: Structure, Function, and Genetics* **47**, 506 (2002).
- [6] T. Wang, J. Miller, N. S. Wingreen, C. Tang, and K. A. Dill, *Journal of Chemical Physics* **113**, 8329 (2000).
- [7] R. Melin, H. Li, N. S. Wingreen, and C. Tang, *Journal of Chemical Physics* **110**, 1252 (1999).
- [8] H. Cejtin, J. Elder, A. Gottlieb, R. Helling, H. Li, J. Philbin, N. Wingreen, and C. Tang, *Journal of Chemical Physics* **116**, 352 (2002).
- [9] H. Chen, X. Zhou, and Z.-C. Ou-Yang, *Physical Review E* **64**, 041905 (2001).
- [10] A. Irback and E. Sandelin, *Journal of Chemical Physics* **108**, 2245 (1998).
- [11] K. F. Lau and K. A. Dill, *Macromolecules* **22**, 3986 (1989).
- [12] W. Kauzmann, *Adv. Protein Chem.* **14**, 1 (1959).
- [13] H. Li, C. Tang, and N. S. Wingreen, *Physical Review Letters* **79**, 765 (1997).
- [14] R. Helling, H. Li, R. Melin, J. Miller, N. Wingreen, C. Zeng, and C. Tang, *Journal of Molecular Graphics and Modelling* **19**, 157 (2001).
- [15] C. T. Shih, Z. Y. Su, J. F. Gwan, B. L. Hao, C. H. Hsieh, J. L. Lo, and H. C. Lee, *Physical Review Letters* **84**, 386 (2000).
- [16] C. T. Shih, Z. Y. Su, J. F. Gwan, B. L. Hao, C. H. Hsieh, J. L. Lo, and H. C. Lee, *Physical Review E* **65**, 41923 (2002).
- [17] M. P. Allen and D. J. Tildesley, *Computer Simulations of Liquids* (Clarendon, Oxford, 1990).
- [18] P. Hanggi, P. Talkner, and M. Borkovec, *Reviews of Modern Physics* **62**, 251 (1990).
- [19] K. Binder, *Physical Review A* **29**, 341 (1984).
- [20] Y. Sang, M. Dubé, and M. Grant, *Physical Review Letters* **87**, 174301 (2001).

- [21] L. Gunther and B. Barbara, Physical review B **49**, 3926 (1994).
- [22] O. Dudko, A. Filippov, J. Klafter, and M. Urbakh, PNAS **100**, 11378 (2003).
- [23] C. L. Dias, M. Dube, F. Oliveira, and M. Grant, Phys. Rev. E **72**, 011918 (2005).